第32卷 第1期　　焊　接　学　报　　Vol.32　No.1
2011年1月　　TRANSACTIONS OF THE CHINA WELDING INSTITUTION　　January　2011

热障涂层的三维界面形貌与热应力关系

王志平，　韩志勇，　陈亚军，　丁坤英

（中国民航大学 材料工艺技术研究所，天津　300300）

王志平

摘　要：使用等离子喷涂方法制备出双层热障涂层（粘结层为 NiCrAlY，陶瓷层为 ZrO_2）．使用 ABAQUS 有限元分析软件，采用间接耦合分析的方法，模拟计算了喷涂过程中陶瓷层/粘结层间三维结构椭圆界面的应力场分布，得出了粘结层表面三维椭球形貌单元位置和尺寸与热应力分布之间的关系．模拟结果表明，涂层制备后，椭球形貌单元位置和尺寸对于陶瓷层和粘结层的界面应力影响较为明显，在形貌单元尺寸一定的情况下，涂层边界附近形貌单元的热应力相对较大，是涂层失效的危险单元，单元角点处为各个单元的危险点，当短半轴为 20 μm 时界面危险点应力 σ_{yy} 达到最大值 324 MPa．

关键词：热障涂层；热应力；界面形貌

中图分类号：TG172.6　文献标识码：A　文章编号：0253－360X（2011）01－0021－04

0　序　言

基于提高航空发动机的经济性和可靠性的要求，热障涂层技术已成为未来发动机热端部件高温防护涂层技术的发展方向[1,2]．由于涂层系统线膨胀系数和导热系数在界面上跃变较大，尤其是在化学组成和物理性能陡变的粘结层和陶瓷层的结合界面上，无论在制备过程中还是在热载荷下，涂层内部的热应力容易导致涂层发生开裂、剥离、脱落等形式的失效．

界面粗糙化可以提高界面的结合强度，粗糙表面有利于增强机械结合力．然而，粗糙化的同时，界面出现复杂形貌，出现的垂直于界面的残余拉应力，可能会导致涂层破裂和剥离[3,4]．

喷涂过程中残余应力与界面形貌的研究与预测的试验研究相对复杂，随着计算机技术的发展，有限元分析方法在分析涂层表面形貌与残余应力关系的研究得到了较快的发展[5,6]．

考虑到涂层制备过程中出现的复杂的三维界面形貌，文中使用 ABAQUS 有限元分析软件，研究了热障涂层制备过程中分界面上典型的三维椭球微坑形貌单元的热应力，对涂层的危险位置和可能的失效方式进行了初步分析．

1　热应力计算的基本原理

当涂层的温度发生变化时，由于热变形而产生线应变 $\alpha(T_1-T_0)$，其中 α 是材料的线膨胀系数，T_1 是弹性体内任一点现时的温度值，T_0 是初始温度值．如果物体的热变形不受任何约束时，则物体上有变形而不引起应力．但是，物体由于约束或各部分温度变化不均匀，热变形不能自由进行时，则在物体中产生应力．

涂层应力计算的过程一般可以分成以下几个步骤．首先根据定解方程 $\lambda\nabla^2T=\rho c_p\,\partial T/\partial t$ 以及模型的初始条件和边界条件计算出涂层冷却过程中的温度场分布，其中 λ 为热导率；ρ 为密度；c_p 为比热容；T 为温度；t 为时间．再根据涂层温度场分布和各部分的线膨胀系数计算在特定约束条件下的变形，然后利用几何方程由变形位移计算涂层各点的应变，最后根据材料的物理方程（应力与应变的关系）由应变计算各点的应力．

2　计算模型的建立

文中的研究对象为等离子喷涂方法制备的双层热障涂层，其陶瓷层（内含质量分数 8% Y_2O_3 的 ZrO_2）厚度为 250 μm，粘结层（Ni-22Cr-10Al-1Y）厚度为 100 μm．粘结层表面均匀分布着椭球形微坑，长半轴长度为 100 μm，短半轴长度的变化范围为 0～50 μm．

收稿日期：2010－03－30
基金项目：国家自然科学基金资助项目（60879018）

由于基体的厚度尺寸远远大于粘结层和陶瓷层的厚度尺寸，分界面为平面时，残余应力最大值在陶瓷层和粘接层的界面上[7]，故计算模型只取粘接层和陶瓷层. 由于对称性，为了节省计算时间同时保证计算结果的准确性，取 1/4体进行分析，取中心形貌单元法向轴线为中心对称轴，模型中水平 xOz平面内取三个周期单元. 粘结层的表面椭球微坑形貌和位置分布如图 1所示. 按照单元分布距离中心轴线位置的远近，分别标号为 1号 ~6号. 整个涂层的网格划分如图 2所示. 计算过程中，采用三维八节点实体减缩积分单元（C3D8R）来计算模拟.

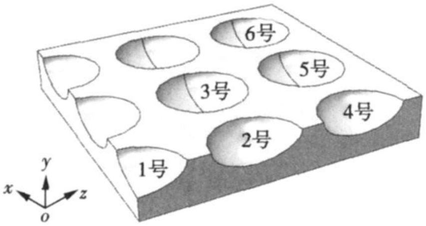

图 1 1/4 粘结层的表面模型

Fig. 1 Schematic of 1/4 part of bond coating surface

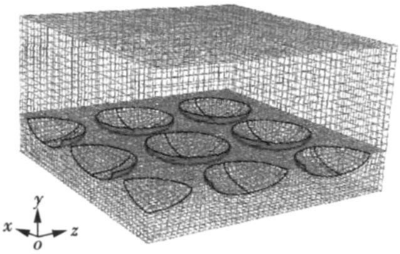

图 2 模型的网格划分

Fig. 2 Mesh of model

热障涂层在制备结束高温阶段，基体和粘接层金属会发生蠕变，可以假定在冷却之前涂层处于应力自由状态. 由热分析[8]知，涂层内的降温幅度和涂层的厚度成正比，同时，由于涂层厚度相对较小，可以近似认为系统在高温 1 000 ℃无应力状态时为均匀的温度场，冷却时温度均匀下降直至冷却终止状态（室温 25 ℃）. 在整个计算过程中涂层周围空间中的温度分布是均衡的，最终的结果与过程无关，只考虑初末两种状态. 由于对称性，xOy面和 yOz面实行对称约束. 由于计算中没有考虑基体，模型中假定粘结层底部为完全固定. 此外，建立有限元模型时，作了如下假设：整个涂层系统没有缺陷；陶瓷层和粘结层在界面处为完全粘结；在降温过程中，涂层系统不产生塑性变形和蠕变，所有的材料属性都是完全弹性的；每层材料内各向同性，并忽略由于温度变化引起的涂层物性参数的变化，其物性参数如表 1[9,10]所示.

表 1 陶瓷层和结合层的热力学参数

Table 1 Thermodynamics parameters of ceramic coating and bond coating

参数	密度 ρ/(kg·m^{-3})	定压比热容 c_p/(J·kg^{-1}·m^{-1})	弹性模量 E/GPa	线膨胀系数 α/(10^{-6}K^{-1})	泊松比 ν(%)
陶瓷层	5 700	565	50	10	0.1
粘结层	7 320	583	200	15.2	0.3

3 计算结果与讨论

3.1 计算结果

取平行于界面方向为 x,z方向，垂直于界面方向为 y方向. 椭圆长半轴为 100 μm，短半轴为 10 μm，yOz平面的应力云图如图 3所示，单个形貌单元相对于涂层中心轴线具有轴对称性，椭圆界面纵切面曲线上均匀取 17个点，令形貌单元最低处横坐标为零，各个椭圆形貌单元计算路径上各个点的 σ_{yy}，σ_{zz}分别如图 4，图 5所示. 由于垂直于界面的残余拉应力 σ_{yy}和平行于界面的压应力 σ_{zz}是导致涂层破坏的主要原因，由图 4和图 5可以看出，在形貌尺寸

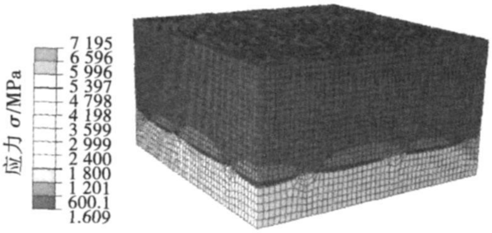

图 3 涂层的热应力分布

Fig. 3 Distribution of thermal stress of coating

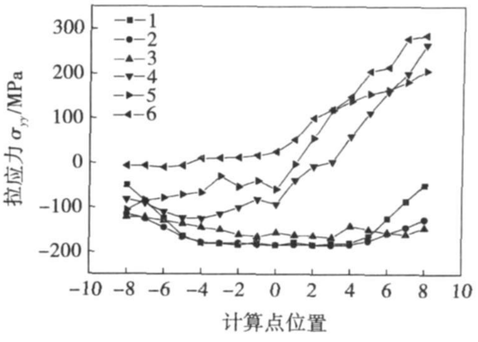

图 4 σ_{yy}随计算路径的变化曲线

Fig. 4 Curves of σ_{yy} changing with calculation path

一定的情况下，残余应力对于形貌单元本身不具有对称性，对于每个形貌单元，距离中心轴线最远位置处的拉应力 σ_{yy}最大，是涂层失效的危险点．为了分析粘结层表面椭球形貌尺寸对热应力的影响，计算了各个形貌单元危险点处 σ_{yy}大小与短半轴长度的变化关系．取椭圆长半轴为 100 μm，短半轴变化范围为 0～50 μm，危险点处的 σ_{yy}随短半轴长度变化规律如图 6所示．

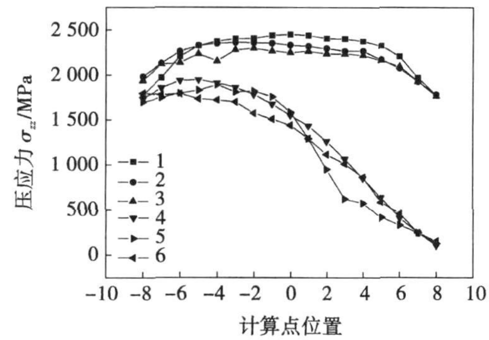

图 5　σ_{zz}随计算路径的变化曲线

Fig. 5　Curves of σ_{zz} changing with calculation path

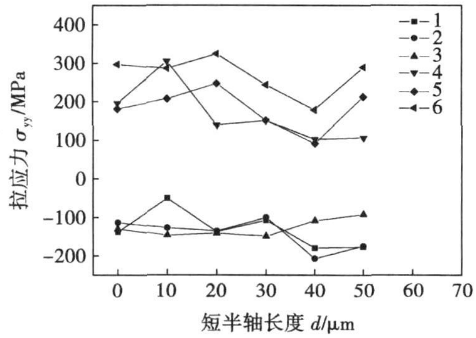

图 6　形貌尺寸对危险点 σ_{yy}的影响规律曲线

Fig. 6　Curves of σ_{yy} changing with danger point

3.2　分析讨论

由图 3可以看出，陶瓷层与粘结层的结合面是应力集中区，存在着应力突变，并且粘结层的等效应力大于陶瓷层的等效应力．这是由于涂层在冷却过程中，陶瓷层和粘结层线膨胀系数不匹配（表 1），导致在交界处有应力集中现象，应力集中的消除是将来重点解决的问题．图 4显示，在椭球微坑形貌单元尺寸一定的情况下，涂层边界附近的 4号～6号单元的垂直界面拉应力 σ_{yy}较大，拉应力基本随着距离中心位置的增加而增大．除 1号单元具有明显对称性外，其它各个形貌单元的热应力不是对称分布，在计算路径的 17个计算点上，σ_{yy}随距离涂层中心轴线距离的变化规律基本一致，σ_{yy}开始基本为压应力，随着距离的增加，压应力变为了拉应力，6号单元的最大拉应力达到了最大值 286 MPa．图 5显示 σ_{zz}始终为拉应力，距离中心轴线较近 1号～3号单元的分布基本为对称分布，涂层边界的 4号～6号形貌单元计算路径上的 σ_{zz}基本随着距离中心位置的增加而减小，且数值较大．这主要是由于建模过程中，考虑到了实际工况，设定的粘结层底面的边界条件为完全固定，导致冷却过程中，限制了粘结层的底面收缩，导致计算结果相对较大．由图 6可以看出，形貌单元的尺寸对于热应力分布的影响比较明显．在横向尺寸固定情况下（100 μm），随着椭球短半轴的增加，危险点的 σ_{yy}变化规律较为复杂，当短半轴长度达到 20 μm时，6号单元的最大拉应力达到最大值 324 MPa，此时，热障涂层最易失效．

4　结　　论

（1）对于双层热障涂层，粘结层表面的三维椭球形貌对陶瓷层/粘结层的界面热应力分布有明显的影响．单元尺寸一定的情况下，涂层边界附近形貌单元的热应力相对较大，是容易失效的危险单元．

（2）对于每个形貌单元，热应力分布不对称，最大值出现在位于距离涂层中心轴线的最远处，是涂层失效的危险点．

（3）椭球形貌长轴固定为 100 μm，短半轴为 20 μm时，危险点拉应力 σ_{yy}最大，可以达到 324 MPa．

参考文献：

[1] Pirge G, Koc I, Basaran A. On the application possibility of thermal barrier coatings in space practices[C] // Proceedings of the 3rd Internal Conference on Recent Advances in Space Technologies, 2007: 152－157.

[2] Xu Yingqiang, Li Shijie, Jin Shaojie. Simulation of interfacial stress in TBCs with oxidation-resistance interlayer under thermal loading[C] // 2009 Second International Conference on Information and Computing Science, 2009: 296－299.

[3] 张红松，王富耻，马　壮．等离子喷涂 ZrO_2 热障涂层的热冲击性能[J]．机械工程材料，2007，31（1）：86－89.
Zhang Hongsong, Wang Fuchi, Ma Zhuang. Thermal shock resistance of plasma-sprayed ZrO_2 thermal barrier coatings[J]. Materials for Mechanical Engineering, 2007, 31(1): 86－89.

[4] Karlsson A M, Hutchinson J W, Evans A G. A fundamental model of cyclic instabilities in thermal barrier systems[J]. Journal of the Mechanics and Physics of Solids, 2002, 50: 1565－1589.

[5] 姚国凤，马红梅，王晓英．热障涂层界面形貌尺寸与残余应力的关系[J]．金属热处理，2005，30(10)，43－46.

Yao Guofeng, Ma Hongmei, Wang Xiaoying. Relation between interface topography dimension and residual stress in themal barrier Coatings[J]. Heat Treatment of Metals, 2005, 30(10), 43−46.

[6] 丁艳霞. 热障涂层中界面形貌对涂层系统中应力影响的研究[D]. 吉林: 吉林大学, 2007.

[7] 徐颖强, 汪震隆, 李剑锋. 含抗氧化夹层热障涂层界面应力特性的研究[J]. 机械强度, 2009, 31(4): 685−688.
Xu Yingqiang, Wang Zhenlong, Li Jianfeng. Investigation of interfacal stress in the temal barrier coatings with oxidation-resistance interlayer[J]. Journal of Mechanical Strength, 2009, 31(4): 685−688.

[8] 王桂兰, 胡帮友, 严　波. 三维等离子喷涂的涂层生长过程温度场数值模拟[J]. 固体力学学报, 2005, 26(2), 151−156.
Wang Guilan, Hu Bangyou, Yan Bo. Numerical simulation of temperature field in forming process of 3D plasma spray coating[J]. Acta Mechanica Solida Sinica, 2005, 26(2): 151−156.

[9] Jinnestrand M, Sjostrom S. Investigation by 3D FE simulations of desalination crack initiation in TBC caused by alumina growth[J]. Surface and Coatings Technology, 2001, B5(2−3), 188−195.

[10] Sfar K, Aktaa J, Munz D. Numerical investigations of residual stress fields and crack behavior in TBC systems[J]. Materials Science and Engineering, 2002, 333: 351−360.

作者简介：王志平, 男, 1963 年出生, 博士, 教授, 硕士生导师. 主要研究方向为热喷涂和焊接技术. 发表论文 20余篇. Email: zpwang@cauc.edu.cn anyong[2], WANG Qing, DAI Zhen[3] (1. School of Material Science and Engineering, Tianjin University, Tianjin 300072, China; 2. Tianjin Key Laboratory of Advanced Joining Technology, Tianjin 300072, China; 3. Hebei Electric Power Research Institute, Shijiazhuang 050021, China). p16—20

Abstract: Type IV cracking is considered to be the likely failure mode of P92 steel welds when operated at high temperature for long duration. Type IV failure often takes place at the intercritical heat affected zone (ICHAZ) or fine grained heat affected zone (FGHAZ). However, the mechanism of type IV cracking has not yet been understood unequivocally. In order to investigate type IV failure scientifically, temperature field, welding residual stress and creep strain for welded joint of P92 steel are simulated by ABAQUS code. Experimental result obtained from X-ray diffraction technique is conducted to verify the simulation. The research results show that the locations of ICHAZ and FGHAZ are demonstrated according to the simulation of temperature field. Maximal residual stress concentrates in the ICHAZ and FGHAZ. And axial creep strain is in good agreement with residual stress. So concentration of residual stress that results in accumulation of creep strain and type IV cracking is regarded as remarkable factor.

Key words: P92 steel; type IV cracking; temperature field; welding residual stress; finite element simulation

Relations between 3-dimension interface topography with thermal stress of thermal barrier coatings WANG Zhiping, HAN Zhiyong, CHEN Yajun, DING Kunying (Institute of Material Technology, Civil Aviation University of China, Tianjin 300300, China). p21—24

Abstract: Double layer thermal barrier coatings (bond coating is NiCrAlY and ceramic coating is ZrO_2) was prepared by atmospheric plasma sprayed method. Using ABAQUS software, the thermal stress distribution of 3-dimension ellipse interface topography between bond coating and ceramic coating was numerically simulated by indirect coupling method. Relations between thermal stress with location and size of ellipse topography unit were obtained. The calculating results show that the stress is affected by location and size obviously and stress of boundary topography unit is bigger than that of center unit when the size of unit is invariable. The boundary topography units are danger unit and corner points are danger points. The stress of danger point reaches 324 MPa when short half axes is 20.

Key words: thermal barrier coatings; thermal stress; interface topography

Master-slave coordinated motion controlling of double-sided arc welding robots ZHANG Huajun[1,3], ZHANG Guangjun[2], CAI Chunbo[2], XIAO Jun[2], GAO Hongming (1. School of Materials Science and Engineering, Harbin University of Science and Technology, Harbin 150040, China; 2. State Key Laboratory of Advanced Welding Production Technology, Harbin Institute of Technology, Harbin 150001, China; 3. School of Material Science and Technology, Shanghai Jiaotong University, Shanghai 200240, China). p25—28

Abstract: A flexible manufacturing system of non root chipping double-sided arc welding robots is studied in order to realize robot automatic welding for thick plate of low alloy high tensile steel. Master-slave coordinated method is adopted. Motoman robot is master and KUKA robot is slave. According to the ending position attitude of welding torch of master hand, reference path plane of plate is look on as symmetric plane. Motion path of slave-hand is deduced by kinematics coordinate conversion. And Master-slave coordinated motion of double-sided arc welding robots is reached and is verified by coordinated motion experiment.

Key words: double-sided arc welding; double robots; master-slave control; coordinated motion

Comprehensive evaluation on effect of weld shape on mechanical performances by analytic hierarchy process LIU Xin[1,2], LEI Yongping, GONG Shuili (1. Beijing University of Technology, Beijing 100010, China; 2. Science and Technology on Power Beam Processes Laboratory, Beijing Aeronautical Manufacturing Technology Research Institute, Beijing 100024, China). p29—32

Abstract: Four different weld shapes are obtained by proper electron beam welding parameters, which are respectively named as bell shape, funnel shape, nail shape and wedge shape. Mechanical performance of the electron beam welded joints with different shapes were carried. The influence of weld shape on mechanical performance of the joints was synthetically evaluated by analytic hierarchy mathematical model. The results show that weld shape effects tensile property, fatigue property and microhardness of the joint. The sequencing of mechanical performance of the joints with four different shapes by analytic hierarchy process is bell shape, funnel shape, wedge shape, and nail shape. It is validated by experimental results that the analytic hierarchy mathematical model is effective and practical.

Key words: weld shape; electron beam welding; mechanical performance; analytic hierarchy process

Effects of welding parameters on weld geometry of pulsed Nd:YAG laser/TIG hybrid welding process of 304 stainless steel ZHANG Linjie[1], ZHANG Jianxun[1], CAO Weijie[1], CHAI Guoming[1], GONG Shuili[2] (1. State Key Laboratory of Mechanical Behavior for Materials, Xi'an Jiaotong University, Xi'an 710049, China; 2. National key Laboratory for High Energy Density Beam Processing Technology, Beijing Aeronautical Manufacturing Technology Research Institute, Beijing 100024, China). p33—36

Abstract: Effects of welding parameters on the weld geometry are investigated for pulsed Nd:YAG laser/TIG hybrid welding of 304 stainless steel plate. The results show that cross sectional area of hybrid weld is larger than the sum of cross sectional area of single laser weld and that of single TIG weld, which means synergetic effect occurs during hybrid welding process; weld width, weld depth, weld cross sectional area and heat transfer efficiency increase with the increase of laser power; when defocusing distance increase from -3mm to 5mm, weld width, weld depth, weld cross sectional area and heat transfer efficiency would increase and reach the maximum when defocus-